Towards achieving high areal capacity in silicon based solid state battery anode: what influences the rate-performance?

Moumita Rana,^{1,*} Yannik Rudel,¹ Philip Heuer,¹ Eva Schlautmann,¹ Carolin Rosenbach,¹ Md Yusuf Ali,² Hartmut Wiggers, ^{2,3} Anja Bielefeld,^{4,5,*} Wolfgang G. Zeier^{1,6,*}

¹Institute of Inorganic and Analytical Chemistry, University of Münster, Corrensstrasse 28/30, 48149

Münster, Germany

²EMPI, Institute for Energy and Materials Processes – Reactive Fluids and

³CENIDE, Center for Nanointegration Duisburg-Essen, University of Duisburg-Essen,

Carl-Benz-Straβe 199, 47057Duisburg, Germany

⁴Center for Materials Research, Justus Liebig University, Heinrich-Buff-Ring 17, 35392 Giessen,

Germany

⁵Institute for Physical Chemistry, Justus-Liebig-University Giessen, Heinrich-Buff-Ring 17, 35392 Giessen, Germany

⁶Institut für Energie- und Klimaforschung, IEK-12: Helmholtz-Institut Münster, Forschungszentrum

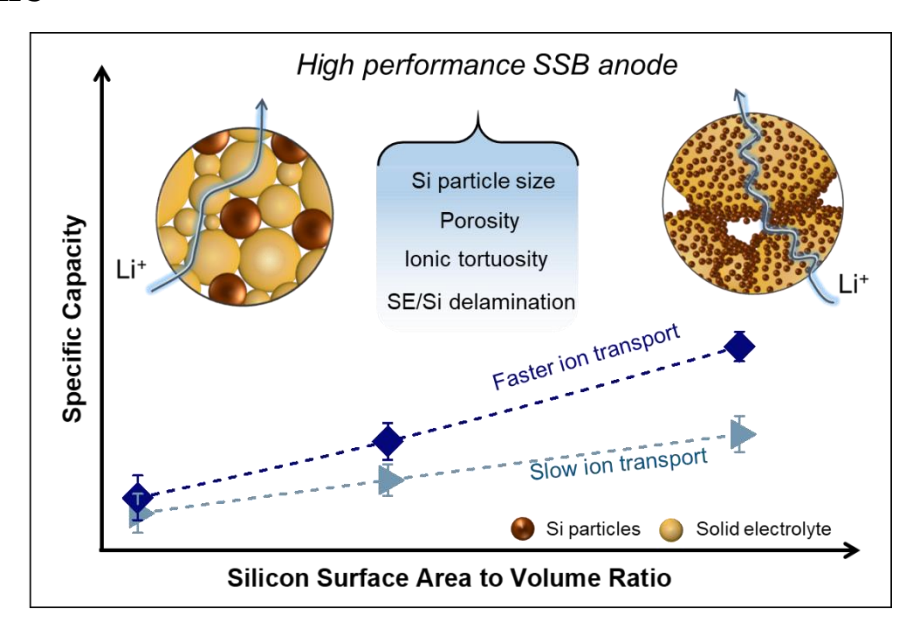
Jülich, Corrensstrasse 46, Münster 48149, Germany

AUTHOR INFORMATION

Corresponding Authors

*rana@uni-muenster.de, * anja.bielefeld@phys.chemie.uni-giessen.de, * wzeier@unimuenster.de ABSTRACT. Achieving high areal capacity and rate performance in solid-state battery electrodes is challenging due to sluggish charge carrier transport through thick all solid composite electrodes, as the transport strongly relies on the microstructure and porosity of the compressed composite. Introducing a high-capacity material like silicon for such purpose would require fast ionic and electronic transport throughout the electrode. In this work, by designing a composite electrode containing Si-nanoparticles, a superionic solid-electrolyte and carbon additive, the possibility of achieving areal capacities over 10 mAh·cm⁻² and 4 mAh·cm⁻² at current densities of 1.6 mA·cm⁻² and 8 mA·cm⁻², respectively, at room temperature is demonstrated. Using DC polarization measurements, impedance spectroscopy, microscopic analyses, and microstructure modelling, we establish that the route to achieve high-performance anode composites is microstructure modulation through attaining high silicon/solid electrolyte interface contacts, particle size compatibility of the composite components, along with their well distributed compact packing in the compressed electrode.

TOC GRAPHIC



Solid-state batteries are promising as the next-generation energy storage system due to their high energy density, wide operating temperature, and volumetric miniaturization. The recent development and understanding of challenges in solid-state batteries (SSB) and further expanding their potential includes improving the areal capacity and power density, which requires development of high-performance solid-state composite electrodes.² Strategies for designing high areal capacity and high-performance electrodes are well investigated for Li-ion batteries with liquid electrolytes, where high specific capacity of the active material,³ faster ion storage kinetics,⁴ enhanced electrochemical surface area with pseudocapacitive ion storage capability, 5,6 and optimized electrode microstructures with optimal electronic conductivity⁷ and porosity⁸ are established to be beneficial. For example, the highest areal capacity achieved for silicon-based electrodes at room temperature is >10 mAh·cm⁻². However, such strategies are not directly translatable for designing high-performance SSB electrodes as the main bottle neck is the restricted ion transport through the composite of the solid electrolyte (SE) and active material. 9-11 Unlike in low capacity materials, attaining high-performance using high capacity materials requires elevated local Li⁺ and electron flux around the active material particles during the charge-discharge process. Therefore, designing a high-performance all-solid electrode requires suitable combination of high capacity active materials, fast ion and electron transport kinetics and favourable low tortuosity pathways. 12,13 While such effects have been investigated for cathode active materials, 12,14,15 no exploration has been shown for high capacity materials such as silicon, towards achieving highperformance anode composites.

Silicon is one of the most promising lithium metal alternatives due to its high theoretical capacity of 3579 mAh·g⁻¹ and low average delithiation potential of 0.4 V vs. Li⁺/Li.^{16,17} Recently, the potential of silicon anodes in the SSB was established through different manufacturing strategies

such as slurry preparation, thin film and composite electrodes.^{17–19} Despite exhibiting strong promises as alternative anode to lithium metal, either such electrodes have shown high-performance at elevated temperature or, are limited by the areal loading of silicon. ^{16,20–22} This can be directly correlated to the limited effective ionic and electronic conductivity in the electrode. On that account, designing high-performance anode composites for room temperature SSB operation requires developing composites with fast effective ionic and electronic conductivities.²³ Considering the Li⁺ transport as the main bottleneck to achieve sufficient effective ionic conductivity of the composite anode, incorporating faster SE into the composite is crucial to attain high-performance. ¹² As the transport of ions and electrons depends on the interfacial contact of the active material with the SE and carbon additive, a higher surface to volume ratio of the active material should be beneficial for building well connected conduction pathways, expected to lead to high-performance behaviour.

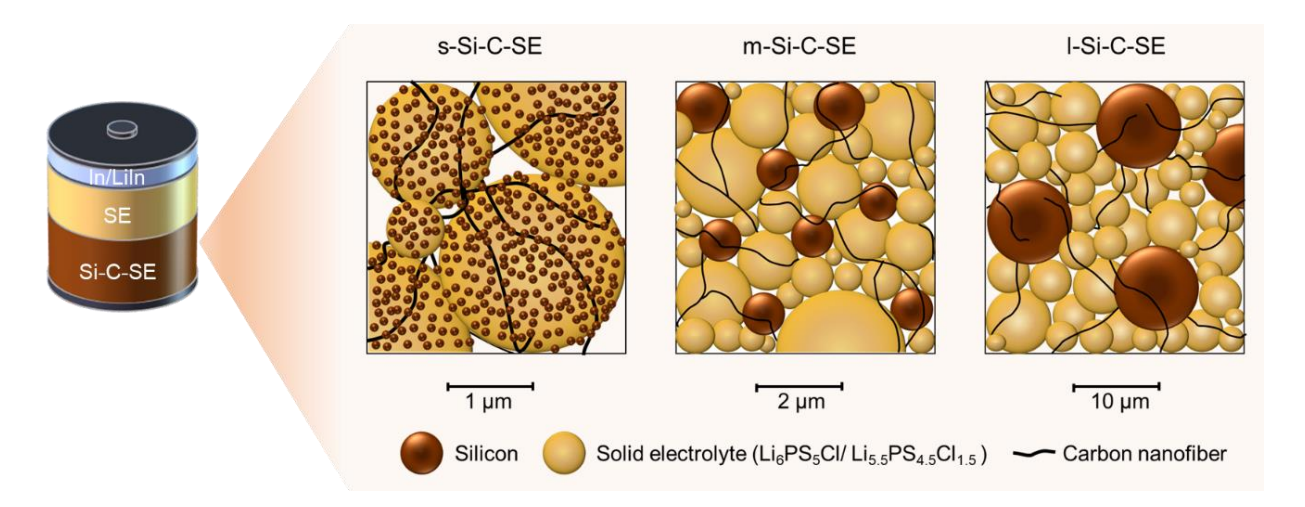


Figure 1. Schematic of the half-cell assembly. The anode composites contain silicon particles (Si, brown spheres), solid electrolyte (SE, beige spheres), and vapor grown carbon nanofibers (C, black line). Three different sizes of the silicon particles are used in the composite: small (s-Si),

medium (m-Si), and large (l-Si). Two different SE, Li₆PS₅Cl and Li_{5.5}PS_{4.5}Cl_{1.5}, are used for the different sets of experiments.

Inspired by the idea of designing high-performance anodes, here silicon-based composites are prepared by combining different sizes of silicon particles with highly conducting SE and vapor grown carbon nanofiber (VGCNF) (Figure 1). To investigate the influence of the silicon particle size on the rate performance of the composite anode, we chose three different silicon particle sizes: 86.6 (± 36.5) nm (small sized, s-Si), 1.36 (± 0.49) μm (medium sized, m-Si) and 9.66 (± 2.83) μm (large sized, 1-Si) as shown in Figure S1. To understand the effect of the ionic conductivity of the SE on the rate performance of the composite anodes, two SE Li₆PS₅Cl and Li_{5.5}PS_{4.5}Cl_{1.5} with ionic conductivities of 3.4 mS·cm⁻¹ and 9.7 mS·cm⁻¹, respectively, are incorporated (Figure S2). The list of composites used for this study is summarized in Table ST1.

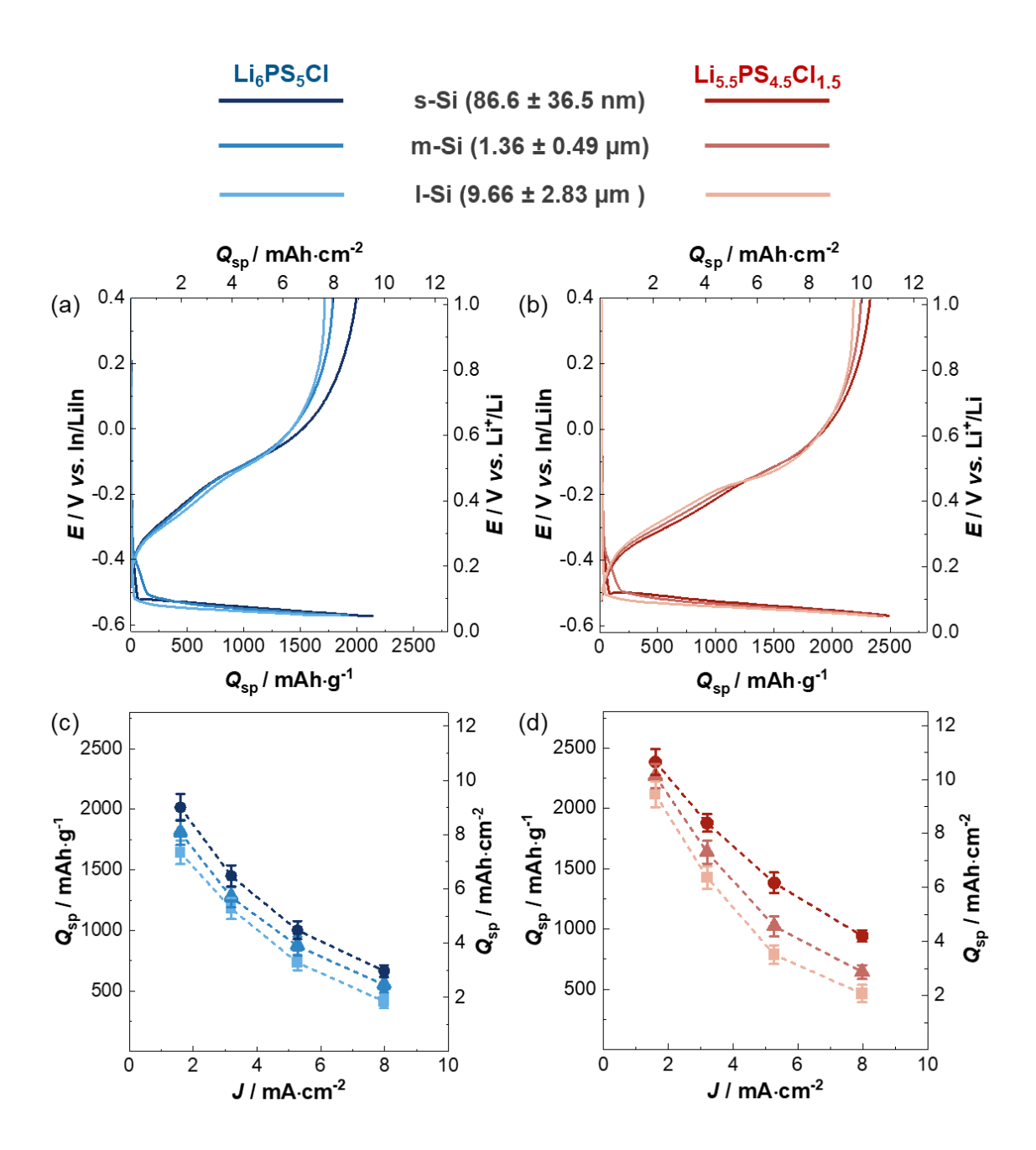


Figure 2. Electrochemical performance of the anode composites containing s-Si, m-Si, and l-Si with Li₆PS₅Cl (blue) and Li_{5.5}PS_{4.5}Cl_{1.5} (red) and VGCNF in half-cell configuration against In/LiIn as the counter electrode. The cells were cycled in the potential range of -0.57 V to 0.4 V vs. In/LiIn at 25°C. Comparison of the potential profiles (a, b) for the 1st charge-discharge cycle at a current density of 1.6 mA·cm⁻², and the rate performance (c, d) of the composite anodes containing (a, c)

Li₆PS₅Cl, and (b, d) Li_{5.5}PS_{4.5}Cl_{1.5} as SE and different sizes of silicon particles. The uncertainties correspond to the variation in three sets of rate capability tests. The specific capacity values are normalized against the silicon content in the composite anode.

Figure 2 shows the comparison of the rate performance of the composites consisting of the s-Si, m-Si and l-Si with Li₆PS₅Cl (now named SE1) and Li_{5.5}PS_{4.5}Cl_{1.5} (now named SE2), respectively. Figure 2 shows the potential profiles of the first charge-discharge cycle of the composites. Figure 2c, d (and Figure S3, S4) show the rate performances of the composites, where the uncertainties correspond to the variability of the specific capacity obtained from triplicated half-cell measurements. An initial Coulomb efficiency of 92 (± 2) % is observed for all half cells. At low current density of 1.6 mA·cm⁻² the composites containing the Li₆PS₅Cl exhibit specific capacities of 8.5 (±0.8) mAh·cm⁻², whereas the composites containing Li_{5.5}PS_{4.5}Cl_{1.5} show specific capacities of 10.85 (±0.4) mAh·cm⁻². As the current density increases, the composites with s-Si and SE2 show the best capacity retention, followed by the ones containing m-Si and l-Si. Even at a very high current of 16 mA·cm⁻² the composites with s-Si, m-Si, and l-Si show specific capacities of 1.54 (± 0.24) , 0.94 (± 0.18) and 0.5 (± 0.13) mAh·cm⁻², respectively (Figure S4). To note, at such high current the composites with SE1 fail to respond to the charge-discharge process (Figure S3). This deciphers that faster Li⁺ transport not only benefits the specific capacity of the composites, also helps improving the rate performance.

The long-term electrochemical stability of these composites was tested using extended galvanostatic charge-discharge for 100 cycles at a current density of 3.2 mA·cm⁻². As shown in the figure S5, the specific capacity retention of the composites containing s-Si, m-Si and l-Si are 64%, 61% and 53% of their initial capacity, respectively. Clearly, the silicon particle size as well as the

type of SE used influences the rate performance of Si based composites. In cathode composites these differences are often assigned to the changes in the partial ionic and partial electronic transport, or composite tortuosity. ¹² Therefore, these parameters need to be explored.

Studying the electronic and ionic transport of the anode composites. First, the dependence of the effective electronic and ionic conductivity, and corresponding tortuosity factors, of these composites on the silicon particle size and SE is investigated (Figure 3, S6-9). Figure 3a shows the average electronic conductivities of the composites containing different silicon particle sizes. The effective electronic conductivity varies in the range of 30 mS·cm⁻¹ to 65 mS·cm⁻¹, and does not differ significantly with the change of the SE.

The tortuosity factor (κ_i) for the effective conductivity of these composites can be estimated using the following equation:

Tortuosity factor,
$$\kappa_i = \frac{\phi_i \cdot \sigma_{0,i}}{\sigma_{eff,i}}$$

where ϕ_i is the volume percentage of the conducting phase, $\sigma_{0,i}$ and $\sigma_{\rm eff,I}$ are the conductivities of the pure conducting phase and effective conductivity of the composite electrode. The index $i \in \{el, ion\}$ refers to the electronic or ionic phase. The electronic tortuosity factors ($\kappa_{\rm el}$) of the composites are estimated against the electronic conductivity of pristine VGCNF, which is $2 \cdot 10^7$ mS·cm⁻¹.²⁴ The $\kappa_{\rm el}$ remain almost similar for all the composites, deciphering that the pathways for electron conduction in these composites are mostly influenced by the presence of the VGCNF.

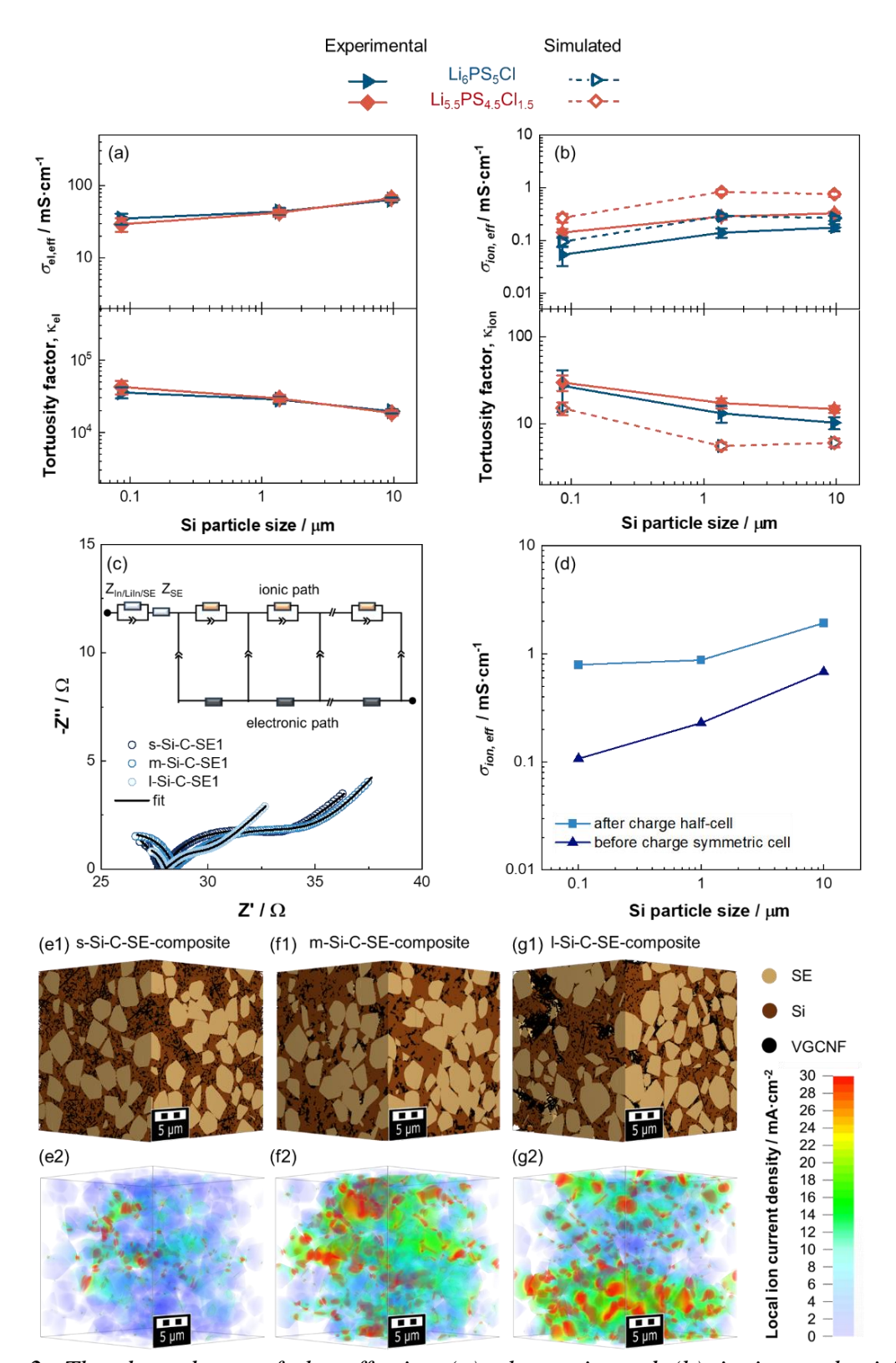


Figure 3. The dependence of the effective (a) electronic and (b) ionic conductivity, and corresponding tortuosity factor on silicon particle size in the composite anodes. The effective

electronic and ionic conductivities of the composites are measured using the ion-blocking and electron blocking cell setup, respectively, and represented by the solid symbols connected with solid lines. The uncertainties correspond to the variation in the results of two sets of polarization experiments. In (b), the open symbols connected with the dashed lines correspond to the simulated effective ionic conductivities and tortuosity factors of the anode composites obtained using the microstructure modelling. (c) Fitted impedance spectra of lithiated (charged) half-cells containing Li₀PS₅Cl as solid electrolyte and corresponding to Z-type transmission line model (inset). (d) Comparison of the effective ionic conductivity of the composites before and after lithiation process. (e-g) Microstructure models (e1, f1, g1) and corresponding current distribution through the compressed composite (e2, f2, g2) from the flux-based simulation for (e) s-Si, (f) m-Si and (g) l-Si-C-SE-composites showing more distributed and higher ionic current (green to orange colour regime) in the anode composites with m-Si and l-Si compared to the one with s-Si.

Figure 3b shows the variation of the effective ionic conductivity of the composites with the silicon particle size and the type of the SE. As the faster Li⁺ conducting Li_{5.5}PS_{4.5}Cl_{1.5} is introduced, the effective ionic conductivity of the composite significantly increases compared to the ones with Li₆PS₅Cl. For example, the mean effective ionic conductivity of the composites containing the s-Si particles are 0.053 ± 0.021 mS·cm⁻¹ and 0.15 ± 0.024 mS·cm⁻¹ for the composites containing Li₆PS₅Cl and Li_{5.5}PS_{4.5}Cl_{1.5}, respectively. We further estimated the effective ionic conductivity values of these composites by applying the T-type transmission line modelling (TLM) on the impedance spectra of the electron blocking cells, ^{14,15,25} which lie in the range and follow the same trend, as shown in the Figures S10d and f. To investigate the change in the effective ionic conductivity of these composites after the lithiation process, we have applied Z-type TLM model for the lithiated (charged) half-cells containing Li₆PS₅Cl as solid electrolyte, as shown in the figure

3c. The overall effective ionic conductivity values of the lithiated composites are found to be significantly higher compared to the as prepared composites (Figure 3d). A detailed discussion and comparison of the conductivity values, obtained from other methods are included in the supporting information.

With increasing size of the silicon particles, the ionic conductivity of the composite slightly increases for both SEs. So far, studies optimizing ionic and electronic transport altered the volume fractions of the SE and strong changes in partial ionic transport of the composite cathodes were observed that could be related to the attainable capacities.^{9,23} A variation in the active material particle size is found to have negligible impact on the effective ionic conductivity of the composite cathode, 26 whereas lowering the SE particle size significantly improved the specific capacity of the cathode composite.²⁷ Here, a considerable influence is observed when changing the silicon particle size, mostly for the smallest particles. To understand this trend, the ionic tortuosity factor can be extracted as well. The composite containing the silicon nanoparticles has the highest κ_{ion} , whereas the tortuosity factor is lower and remains similar for composites with m-Si and l-Si. One may assume that these significant differences in the tortuosity factor can be related to presence of pores in the composites. Apparent density measurements reveal that in the composite containing s-Si, the relative content of pore volume is 20.88 (\pm 1.7) %, whereas for the composites containing m-Si and I-Si the porosity values are 5.77 (\pm 0.32) % and 7.61 (\pm 0.62) %, respectively (Table ST2 in the SI). In order to understand such variation in the porosity of these composites, we investigated their microscopic morphological features. Figure S11 shows the scanning electron micrographs of the SE after mechanical soft milling. A wide distribution of the SE particle size mostly ranging from 3-8 µm was observed. In the composite with s-Si, the silicon nanoparticles adhere onto the SE particles, whereas in the composite containing m-Si and 1-Si, the SE particles remain next to

each other as a physical mixture. When compressed under the high pressure (uniaxial 375 MPa), the composites with compatible size of silicon (m-Si and 1-Si) and SE microparticles undergoes dense packing (as also evident from the post-mortem microscopic analysis of the compressed composite in Figure S15). In these cases, the silicon microparticles can act as filler in the compressed SE matrix, thereby leading to a more condensed packing. In contrast, in absence of such filler phase, the packing of the SE microparticles covered with the silicon nanoparticles is not effective.

To understand the trend of effective ionic conductivity further in these composites, the compressed composites were modelled, and their effective ionic conductivity simulated by composing a solid electrolyte matrix embedding the spherical s-Si or polyhedral m-Si and l-Si, and randomly distributed pores throughout the composites. Ion transport is solely enabled by the pathways that the SE network offers. Comparing the s-Si to the m-Si and l-Si composites, despite the same mass fractions, the SE volume fraction is quite different due to the higher residual porosity in the s-Si composites (40.9 vol% in s-Si composite and 48.6 vol% in m-Si composite, 47.9 vol% in l-Si composite, respectively; see Table ST3). Therefore, the ion transport pathways in the s-Si composites are disturbed by the residual pores which increases the ionic tortuosity factor. In other words, the large size mismatch of the particles in the composites leads to more detrimental pores. This is further investigated by the ionic current distribution in the microstructures using flux-based simulations (Figure 3e-g).

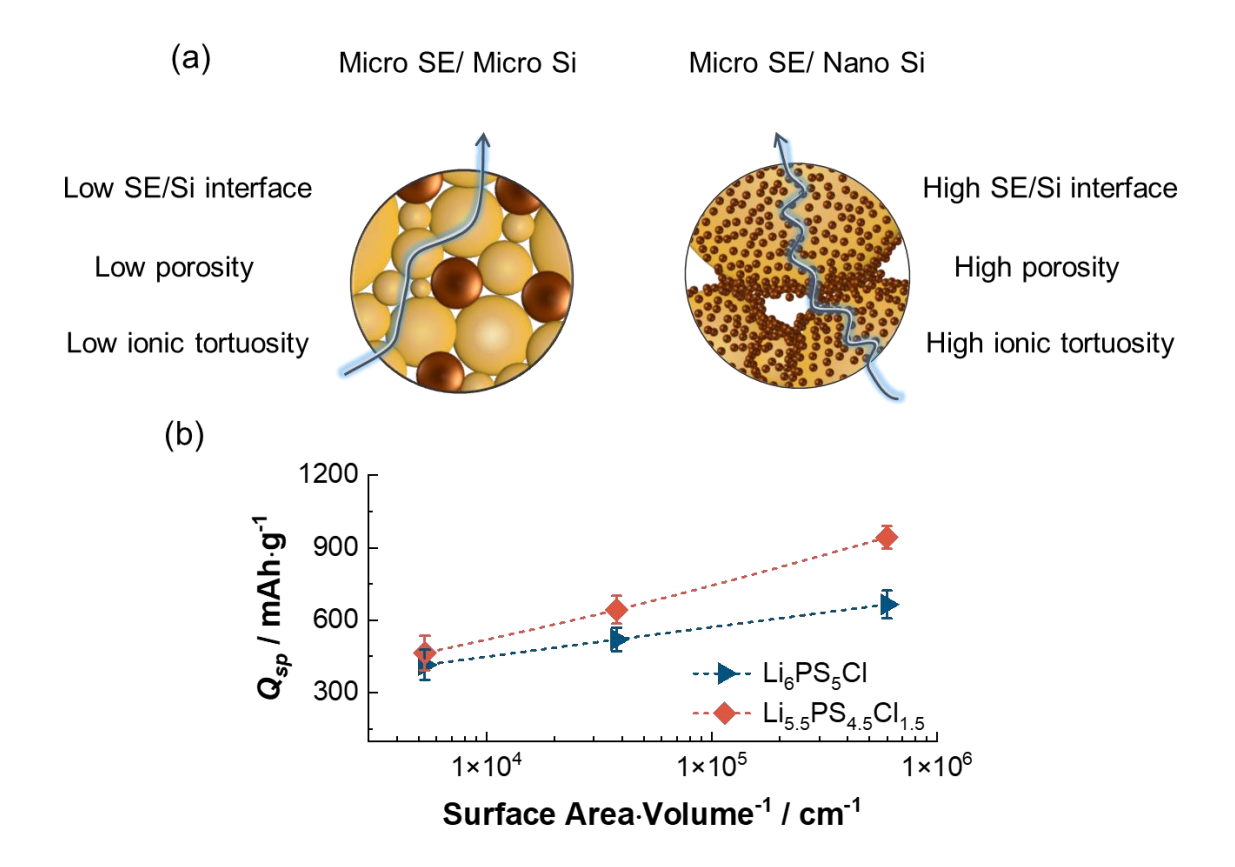


Figure 4. Influence of silicon particle size and ionic conductivity of the solid electrolyte on the rate performance of the anode composites. (a) Schematic showing the similarity in the size of the silicon (m-Si, l-Si) and SE microparticles results in a better packing in the compressed composite, leading to low porosity and ionic tortuosity (left). The size mismatch between the silicon nanoparticles and SE microparticles and the adherence of Si nanoparticles on the SE microparticles creates porosity in the composite, which results in high ionic tortuosity (right). However, the high Si/SE interface in the s-Si composites favors the rate performance. (b) Dependence of the specific capacity of the composites at current density of 8 mA·cm⁻² on the surface area/volume ratio of the silicon particles. The specific capacity increases with higher surface area/volume ratio of the silicon particles. The rate performance of the anode composite

improves with the improved ionic conductivity of the solid electrolyte. The specific capacity values are normalized against the silicon content in the composite anode.

Microstructure models of the different composites and flux-based simulations are reconstructed on these composites in GeoDict, ²⁸ similar to Bielefeld et al. and Park et al. ^{29,30} The simulation setup and the microstructure reconstruction are described in detail in the SI. Figure 3e-g show the microstructure models for composites with different Si particle size as well as their distribution through the SE grains. The estimated effective ionic conductivities of the composites are shown in Figure 3b with the open symbols. As shown in the Figure 3e2-g2, for the composite containing s-Si, the overall ionic current is comparably small and passes through a fraction of the SE grains only. Current focusing on the grain contacts is visible, indicating that with elevated porosity poor inter-grain-contact occurs. Due to more effective packing, the local ion current is better distributed leading to a stronger current flow in the m-Si and l-Si composites over the ones with s-Si. This is reflected in the effective ionic conductivity of 0.27 mS·cm⁻¹ and the ionic tortuosity factor of 15 for the s-Si-C-SE2 composite, displayed in Figure 3. The composites containing m-Si- and the l-Si possess relatively higher effective ionic conductivities of 0.84 and 0.76 mS·cm⁻¹, respectively.

What limits the high-rate performance in Si based composite anode? Overall, from the above observations a few trends seem clear: 1) the electronic conductivities between the composites with different silicon particle sizes and SE only change minor. 2) With changing the SE from Li₆PS₅Cl to Li_{5.5}PS_{4.5}Cl_{1.5}, faster effective ionic transport is observed. This can explain the overall improved rate performance of the cells using Li_{5.5}PS_{4.5}Cl_{1.5}, but not the influence of the particle size. 3) By changing the size of Si particles, the surface to volume ratio of the active material changes. For the electrochemical reaction to occur both ions and electrons need to be transported to the silicon particles, but at the same time enough reaction sites (Si/SE interface) need to be available (Figure

4a). Here, to simplify the comparison, a spherical shape of silicon particles is assumed to calculate their surface to volume ratio from the obtained particle size distributions. Figure 4b shows the dependence of the specific capacity of the composites at current density of 8 mA·cm⁻² for both the electrolytes as a function of the surface to volume ratio of the silicon particles. A correlation of a higher surface to volume ratio is evident that leads to better rate performance. The dependence increases in the presence of the Li_{5.5}PS_{4.5}Cl_{1.5}. The enhanced Si/SE contact area in the composites with smaller silicon particles also leads to more SEI formation due to the degradation of the solid electrolytes, as observed from the postmortem XPS analysis (Figure S17).^{31,32} However, this does not have direct impact on the cycling stability of these materials. Even though the smaller particle size of the silicon favors the rate performance, due to its high surface energy, the silicon nanoparticles adhere to the SE microparticles during the preparation of the composite. 4) This leads the s-Si composites to have a higher porosity, resulting in a more tortuous ion transport pathway. The presence of such high porosity in the pristine and composite silicon nanoparticle based anodes were also observed in a recent study by Cao et al. 22 This infers that the use of nanoparticles as the active material is detrimental for achieving less tortuous ion transport pathway in electrode composites. In contrast, the composites containing m-Si and l-Si have much lower porosity in the compressed state due to 5) compatibility in the particle size of silicon and SE. The presence of such enhanced porosity in the s-Si composites does not benefit the volumetric capacity of the composites containing Li₆PS₅Cl (Figure S18). However, when Li_{5.5}PS_{4.5}Cl_{1.5} is used as the solid electrolyte, faster ion transport favors the overall volumetric capacity. The volumetric capacity values of these composite anodes are in the range of the high-performance electrodes for batteries with liquid electrolytes, and can be further improved through modulating the particle size distribution and improving effective ionic conductivity of the composite. 33–35 Even

though the composites containing the m-Si and l-Si possess higher effective ionic conductivity compared to the composites containing s-Si, 6) they experience mechanochemical failure during the charge-discharge process (Figure S15), that have negative influence on the rate performance. Nevertheless, 7) the influence of much higher Si/SE interface in the s-Si composites on the rate performance compared to the ones with m-Si and l-Si surpasses the impact of the effective ionic conductivity of the composites in presence of the same SE. Overall, the route to high areal capacity and high rate performance in the silicon based composite anodes is by modulation of the microstructure to achieve enhanced Si/SE interface and high effective ionic conductivity.

In conclusion, this study demonstrates a route to achieve high-performance silicon-based anode composites for SSB and investigates the underlying charge carrier transport and microscopic influence involved therein. By varying the particle size of silicon and the ionic conductivity of the SE in the anode composite and analyzing their electrochemical performance and charge carrier transport, we found that an enhanced surface to volume ratio of active material particle, high effective ionic conductivity, particle size compatibility and homogeneous distribution of the composite ingredients, and low porosity favors the high-performance in the Si based anode composites. This strategy allows accessing 10 mAh·cm⁻² and 4 mAh·cm⁻² of specific capacity at current densities of 1.6 mA·cm⁻² and 8 mA·cm⁻², respectively, at ambient temperature with a combination of silicon nanoparticles and a fast ion conducting electrolyte in a composite electrode. Detailed DC polarization results and microstructural modelling reveal that the particle size compatibility of silicon and SE causes low porosity in the compressed anode composite, that facilitates more uniform distribution of ion flux throughout the SE matrix, thereby improving the effective ionic conductivity of the electrode. Further improvements in the anode composite performance will require optimization of the SE particle size, composite processing and sintering

routes to achieve lower porosity in the electrode without compromising on the effective ionic conductivity, that will facilitate less tortuous and fast ion conduction pathway, and thereby facilitate the high-performance behavior in the electrodes for SSB.

ASSOCIATED CONTENT

Supporting Information. Experimental section, Table of composite composition used for this study. Figure S1. characterization of the solid electrolytes by XRD, Raman, Impedance spectroscopy. Figure S2 includes FESEM images and the particle size distribution analysis of the silicon particles. Figure S3-S4 includes representative rate performance tests, corresponding voltage profiles. Figure S5 shows long term cycling stability profiles of the anode composites. Figure S6-S9 shows the current-voltage response from the DC polarization experiments. Discussion of application of transmission line modelling on the cell impedance and related information in Figure S10. Figure S11-14 show the FESEM images and EDS mapping of the solid electrolyte and the composites before electrochemical cycling. Discussions on chemomechanics of Si composite based anodes including post-mortem FESEM images and EDS mapping of the composites in Figure S15 and S16. XPS spectra of the composites before and after electrochemical cycling is given in Figure S17. Figure S18 shows estimation of volumetric specific capacity of the composites. Details of microstructural simulation methods, development of composite microstructure models, estimation of effective ionic conductivity, included in Figure S19-S21.

Notes

The authors declare no competing financial interest.

ACKNOWLEDGMENT

MR acknowledges funding from the Alexander von Humboldt foundation. The authors acknowledge financial support within the SilKompAs funded by Bundesministerium für Bildung und Forschung (BMBF project 03XP0486B).

REFERENCES

- (1) Janek, J.; Zeier, W. G. A Solid Future for Battery Development. *Nat. Energy* **2016**, *1* (9), 16141.
- (2) Janek, J.; Zeier, W. G. Challenges in Speeding up Solid-State Battery Development. *Nat. Energy* **2023**.
- (3) Park, S.-H.; King, P. J.; Tian, R.; Boland, C. S.; Coelho, J.; Zhang, C. (John); McBean, P.; McEvoy, N.; Kremer, M. P.; Daly, D.; Coleman, J. N.; Nicolosi, V. High Areal Capacity Battery Electrodes Enabled by Segregated Nanotube Networks. *Nat. Energy* **2019**.
- (4) Rana, M. Pendashteh, A. Schäufele, R. Gispert, J. Vilatela, J. J. Eliminating Solvents and Polymers in High-Performance Si Anodes by Gas-Phase Assembly of Nanowire Fabrics. *Adv. Energy Mater.* **2022**, 2103469.
- (5) Augustyn, V.; Simon, P.; Dunn, B. Pseudocapacitive Oxide Materials for High-Rate Electrochemical Energy Storage. *Energy Environ. Sci.* **2014**, *7* (5), 1597–1614.
- (6) Rana, M.; Sai Avvaru, V.; Boaretto, N.; de la Peña O'Shea, V. A.; Marcilla, R.; Etacheri, V.; Vilatela, J. J. High Rate Hybrid MnO 2 @CNT Fabric Anodes for Li-Ion Batteries: Properties and a Lithium Storage Mechanism Study by in Situ Synchrotron X-Ray Scattering. J. Mater. Chem. A 2019, 7 (46), 26596–26606.
- (7) Tian, R.; Alcala, N.; O'Neill, S. J. K.; Horvath, D. V; Coelho, J.; Griffin, A. J.; Zhang, Y.;

- Nicolosi, V.; O'Dwyer, C.; Coleman, J. N. Quantifying the Effect of Electronic Conductivity on the Rate Performance of Nanocomposite Battery Electrodes. *ACS Appl. Energy Mater.* **2020**, *3* (3), 2966–2974.
- (8) Jia, H.; Li, X.; Song, J.; Zhang, X.; Luo, L.; He, Y.; Li, B.; Cai, Y.; Hu, S.; Xiao, X.; Wang, C.; Rosso, K. M.; Yi, R.; Patel, R.; Zhang, J.-G. Hierarchical Porous Silicon Structures with Extraordinary Mechanical Strength as High-Performance Lithium-Ion Battery Anodes. *Nat. Commun.* 2020, 11 (1), 1474.
- (9) Bielefeld, A.; Weber, D. A.; Janek, J. Microstructural Modeling of Composite Cathodes for All-Solid-State Batteries. *J. Phys. Chem. C* **2019**, *123* (3), 1626–1634.
- (10) Shi, T.; Tu, Q.; Tian, Y.; Xiao, Y.; Miara, L. J.; Kononova, O.; Ceder, G. High Active Material Loading in All-Solid-State Battery Electrode via Particle Size Optimization. *Adv. Energy Mater.* **2020**, *10* (1), 1902881.
- (11) Zaman, W.; Hatzell, K. B. Processing and Manufacturing of next Generation Lithium-Based All Solid-State Batteries. *Curr. Opin. Solid State Mater. Sci.* **2022**, *26* (4), 101003.
- (12) Minnmann, P.; Strauss, F.; Bielefeld, A.; Ruess, R.; Adelhelm, P.; Burkhardt, S.; Dreyer, S. L.; Trevisanello, E.; Ehrenberg, H.; Brezesinski, T.; Richter, F. H.; Janek, J. Designing Cathodes and Cathode Active Materials for Solid-State Batteries. *Adv. Energy Mater.* 2022, 12 (35), 2201425.
- (13) Jiang, W.; Zhu, X.; Huang, R.; Zhao, S.; Fan, X.; Ling, M.; Liang, C.; Wang, L. Revealing the Design Principles of Ni-Rich Cathodes for All-Solid-State Batteries. *Adv. Energy Mater.* **2022**, *12* (13), 2103473.
- (14) Ohno, S.; Rosenbach, C.; Dewald, G. F.; Janek, J.; Zeier, W. G. Linking Solid Electrolyte Degradation to Charge Carrier Transport in the Thiophosphate-Based Composite Cathode

- toward Solid-State Lithium-Sulfur Batteries. Adv. Funct. Mater. 2021, 31 (18), 2010620.
- (15) Hendriks, T. A.; Lange, M. A.; Kiens, E. M.; Baeumer, C.; Zeier, W. G. Balancing Partial Ionic and Electronic Transport for Optimized Cathode Utilization of High-Voltage LiMn2O4/Li3InCl6 Solid-State Batteries. *Batter. Supercaps* **2023**, *n/a* (n/a), e202200544.
- (16) Tan, D. H. S.; Chen, Y.-T.; Yang, H.; Bao, W.; Sreenarayanan, B.; Doux, J.-M.; Li, W.; Lu, B.; Ham, S.-Y.; Sayahpour, B.; Scharf, J.; Wu, E. A.; Deysher, G.; Han, H. E.; Hah, H. J.; Jeong, H.; Lee, J. B.; Chen, Z.; Meng, Y. S. Carbon-Free High-Loading Silicon Anodes Enabled by Sulfide Solid Electrolytes. *Science* (80-.). 2021, 373 (6562), 1494–1499.
- (17) Lewis, J. A.; Cavallaro, K. A.; Liu, Y.; McDowell, M. T. The Promise of Alloy Anodes for Solid-State Batteries. *Joule* **2022**, *6* (7), 1418–1430.
- (18) Huo, H.; Janek, J. Silicon as Emerging Anode in Solid-State Batteries. *ACS Energy Lett.* **2022**, 7 (11), 4005–4016.
- (19) Cavallaro, K. A.; Sandoval, S. E.; Yoon, S. G.; Thenuwara, A. C.; McDowell, M. T. Low-Temperature Behavior of Alloy Anodes for Lithium-Ion Batteries. *Adv. Energy Mater.* **2022**, *12* (43), 2201584.
- (20) Poetke, S.; Cangaz, S.; Hippauf, F.; Haufe, S.; Dörfler, S.; Althues, H.; Kaskel, S. Partially Lithiated Microscale Silicon Particles as Anode Material for High-Energy Solid-State Lithium-Ion Batteries. *Energy Technol.* **2023**, *n/a* (n/a), 2201330.
- (21) Cangaz, S.; Hippauf, F.; Reuter, F. S.; Doerfler, S.; Abendroth, T.; Althues, H.; Kaskel, S. Enabling High-Energy Solid-State Batteries with Stable Anode Interphase by the Use of Columnar Silicon Anodes. *Adv. Energy Mater.* **2020**, *10* (34), 2001320.
- (22) Cao, D.; Ji, T.; Singh, A.; Bak, S.; Du, Y.; Xiao, X.; Xu, H.; Zhu, J.; Zhu, H. Unveiling the Mechanical and Electrochemical Evolution of Nanosilicon Composite Anodes in Sulfide-

- Based All-Solid-State Batteries. Adv. Energy Mater. 2023, n/a (n/a), 2203969.
- (23) Dewald, G. F.; Ohno, S.; Hering, J. G. C.; Janek, J.; Zeier, W. G. Analysis of Charge Carrier Transport Toward Optimized Cathode Composites for All-Solid-State Li–S Batteries. *Batter. Supercaps* **2021**, *4* (1), 183–194.
- (24) Endo, M.; Koyama, T.; Hishiyama, Y. Structural Improvement of Carbon Fibers Prepared from Benzene. *Jpn. J. Appl. Phys.* **1976**, *15* (11), 2073.
- (25) Siroma, Z.; Sato, T.; Takeuchi, T.; Nagai, R.; Ota, A.; Ioroi, T. AC Impedance Analysis of Ionic and Electronic Conductivities in Electrode Mixture Layers for an All-Solid-State Lithium-Ion Battery. J. Power Sources 2016, 316, 215–223.
- (26) Strauss, F.; Bartsch, T.; de Biasi, L.; Kim, A.-Y.; Janek, J.; Hartmann, P.; Brezesinski, T. Impact of Cathode Material Particle Size on the Capacity of Bulk-Type All-Solid-State Batteries. *ACS Energy Lett.* **2018**, *3* (4), 992–996.
- (27) Cronau, M.; Duchardt, M.; Szabo, M.; Roling, B. Ionic Conductivity versus Particle Size of Ball-Milled Sulfide-Based Solid Electrolytes: Strategy Towards Optimized Composite Cathode Performance in All-Solid-State Batteries. *Batter. Supercaps* 2022, 5 (6), e202200041.
- (28) Math2Market GmbH, GeoDict The Digital Material Laboratory, Version 2022 SP 3, 2022.
- (29) Bielefeld, A.; Weber, D. A.; Janek, J. Modeling Effective Ionic Conductivity and Binder Influence in Composite Cathodes for All-Solid-State Batteries. *ACS Appl. Mater. Interfaces* **2020**, *12* (11), 12821–12833.
- (30) Park, J.; Kim, K. T.; Oh, D. Y.; Jin, D.; Kim, D.; Jung, Y. S.; Lee, Y. M. Digital Twin-Driven All-Solid-State Battery: Unraveling the Physical and Electrochemical Behaviors. *Adv. Energy Mater.* **2020**, *10* (35), 2001563.

- (31) Wenzel, S.; Sedlmaier, S. J.; Dietrich, C.; Zeier, W. G.; Janek, J. Interfacial Reactivity and Interphase Growth of Argyrodite Solid Electrolytes at Lithium Metal Electrodes. *Solid State Ionics* **2018**, *318*, 102–112.
- (32) Wang, S.; Tang, M.; Zhang, Q.; Li, B.; Ohno, S.; Walther, F.; Pan, R.; Xu, X.; Xin, C.; Zhang, W.; Li, L.; Shen, Y.; Richter, F. H.; Janek, J.; Nan, C.-W. Lithium Argyrodite as Solid Electrolyte and Cathode Precursor for Solid-State Batteries with Long Cycle Life. *Adv. Energy Mater.* **2021**, *11* (31), 2101370.
- (33) Liang, J.; Xiao, K.; Fang, R.; Rawal, A.; Lennon, A.; Wang, D.-W. High Volumetric Capacity Nanoparticle Electrodes Enabled by Nanofluidic Fillers. *Energy Storage Mater*. **2021**, *43*, 202–211.
- (34) Gueon, D.; Ju, M.-Y.; Moon, J. H. Complete Encapsulation of Sulfur through Interfacial Energy Control of Sulfur Solutions for High-Performance Li–S Batteries. *Proc. Natl. Acad. Sci.* **2020**, *117* (23), 12686–12692.
- (35) Jain, R.; Lakhnot, A. S.; Bhimani, K.; Sharma, S.; Mahajani, V.; Panchal, R. A.; Kamble, M.; Han, F.; Wang, C.; Koratkar, N. Nanostructuring versus Microstructuring in Battery Electrodes. *Nat. Rev. Mater.* 2022, 7 (9), 736–746.